Design and verification of a simple 3D dynamic model of speed skating which mimics observed forces and motions

van der Kruk, E.; Veeger, H. E.J.; van der Helm, F. C.T.; Schwab, A. L.

DOI
10.1016/j.jbiomech.2017.09.004

Publication date
2017

Document Version
Final published version

Published in
Journal of Biomechanics

Citation (APA)
van der Kruk, E., Veeger, H. E. J., van der Helm, F. C. T., & Schwab, A. L. (2017). Design and verification of a simple 3D dynamic model of speed skating which mimics observed forces and motions. *Journal of Biomechanics*, *64*, 93-102. https://doi.org/10.1016/j.jbiomech.2017.09.004

Journal of Biomechanics 64 (2017) 93–102

Contents lists available at ScienceDirect

Journal of Biomechanics

journal homepage: www.elsevier.com/locate/jbiomech
www.JBiomech.com

Design and verification of a simple 3D dynamic model of speed skating which mimics observed forces and motions

E. van der Kruk *, H.E.J. Veeger, F.C.T. van der Helm, A.L. Schwab

Department of Biomechanical Engineering, Delft University of Technology, Mekelweg 2, Delft, The Netherlands

ARTICLE INFO

Article history:
Accepted 4 September 2017

Keywords:
Multibody model
Speed skating
Optimization
Verification

ABSTRACT

Advice about the optimal coordination pattern for an individual speed skater, could be addressed by simulation and optimization of a biomechanical speed skating model. But before getting to this optimization approach one needs a model that can reasonably match observed behaviour. Therefore, the objective of this study is to present a verified three dimensional inverse skater model with minimal complexity, which models the speed skating motion on the straights. The model simulates the upper body transverse translation of the skater together with the forces exerted by the skates on the ice. The input of the model is the changing distance between the upper body and the skate, referred to as the leg extension (Euclidean distance in 3 D space). Verification shows that the model mimics the observed forces and motions well. The model is most accurate for the position and velocity estimation (respectively 1.2% and 2.9% maximum residuals) and least accurate for the force estimations (underestimation of 4.5–10%). The model can be used to further investigate variables in the skating motion. For this, the input of the model, the leg extension, can be optimized to obtain a maximal forward velocity of the upper body.

1. Introduction

Speed skaters can only push-off laterally to their blade, therefore they are restricted to a specific motion pattern. A skating stroke during speed skating the straights can be divided into three phases: the glide phase, the push-off phase and the re-position phase (Fig. 1) (Van Ingen Schenau, 1981). During the glide phase, the mass of the skater is supported over one leg, whereby the ankle-hip distance remains more or less constant. The skater then starts to increase this distance by introducing a leg extension, thereby moving the center of mass away from the skate, which indicates the start of the push-off phase. The push-off phase ends when the leg is at its maximal extension. Since the leg extension velocity can no longer keep up with the upper body velocity in this phase, the skate leaves the ice. During the re-positioning phase the skate is retracted under the body of the skater, until the skater places the skate again on the ice, whereby the glide phase begins, which completes the motion cycle. Double support (both skates on the ice) exists when one leg is at the start of the glide phase while the other leg is at the end of push-off. This coordination pattern results in a sinus-wave like transverse trajectory of the upper body over the ice.

Within the restriction of this motion, still a distinct difference in coordination patterns among (elite) speed skaters is observed. This indicates room for individual optimization of the speed skating motion. Finding this optimal coordination pattern could well be addressed by simulation and optimization of a biomechanical model of speed skating. But before getting to this optimization approach one needs a model that can reasonably match observed behaviour.

Currently, there are two speed skating models describing the coordination patterns of skaters. First, there is a dynamic model, consisting of 19 rigid bodies and 160 muscles, which can simulate the speed skating motion and gives insight in the forces and motions acting in the joints (Otten, 2003); Second, there is an inverse dynamic model of a speed skater of Allinger & Bogert (1997), which is driven by individual strokes and gives insight in the coordination pattern of the speed skater. To the best knowledge of the authors, both models have not been validated with actual (force) measurements, nor were the effects of the assumptions investigated. Furthermore, the application of the model by Allinger & Bogert (1997) is limited, since it is driven by a presumed function in time rather than measured leg extensions and the body height was assumed constant. Apart from speed skating, there is one other skating model developed, simulating the skating push-off force in cross-country skiing (Bruzzo et al., 2016). This is a multibody model of a two-segment leg (with the upper body mass

* Corresponding author.
E-mail address: e.vanderkruk@tudelft.nl (E. van der Kruk).

http://dx.doi.org/10.1016/j.jbiomech.2017.09.004
0021-9290/

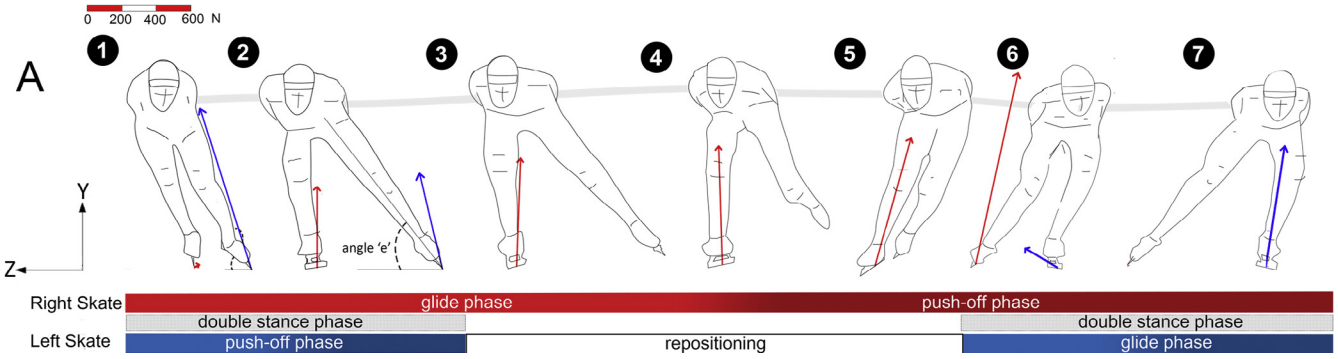

Fig. 1. Phases in the skating motion; the figure is adopted from (van der Kruk et al., 2017). Skating is divided into the four phases: glide phase, push off phase, repositioning phase and the double stance, where both skates are on the ice. The push-off angle of the leg is the angle the leg makes with the horizontal during the push-off motion in the frontal plane. The arrows indicate the push-off force in global space, the scale is indicate in the top-right corner. The grey line indicates the CoM motion of the HAT.

attached to the top of the leg), using the orientation of each leg segment as input for their simulation. The aim of their model was to estimate the push-off force rather than a model which could be used for technique optimization. Thus although (speed) skating models have been developed, none of them have been shown to accurately predict the observed coordination pattern.

The objectives of this study are to present a verified three dimensional dynamic skater model with minimal complexity – built on previous work in rowing (Cabrera et al. (2006)) and speed skating (Fintelman et al., 2011; van der Kruk et al., 2015) - modelling the speed skating motion on the straights. The model is driven by the leg extension - the changing distance between the upper body and the skate - and the skate steering, which we call motion coordination. In this paper we present the verification of this novel model through correlation with observed kinematics and forces.

2. Methods

2.1. Model description

The skater is considered as a combination of three point masses, which are situated at the upper body (mass B) and at each skate (mass S) (Fig. 2). Since the double stance phase is rather short, it is assumed that there exists no double stance phase. Therefore, only one skate at the time is on the ice, alternating left and right. The point of alternation is defined as the moment in time where the forces exerted on both skates are equal. So at any point in time, only two masses are considered in the model, which we refer to as the *active masses* (mass B and one of the skates). The repositioning phase of the inactive skate in the air is therefore neglected. Each mass has three degrees of freedom. The set of parameters is restricted to the position coordinates of mass B (x_b, y_b, z_b), two translations in the transverse plane of mass S, with the position coordinates (x_s, y_s) (because the skate is assumed to be on the ice, making $z_s = 0$ at all times) and one rotation in the same plane, the steer angle (θ_S). This steer angle is of importance for the constraint forces acting on the skate, since we assume that the skate can only glide in the direction of the blade, restricting lateral slip. All other rotations of the skates and the upper body rotations are neglected. The bodyweight of the skater is distributed over the two active masses by a constant mass distribution coefficient (η). Furthermore, the arm movements are assumed to be of marginal effect on the overall power and are therefore neglected.

The input of the model is the changing distance between the point mass position of the upper body and the skate (Euclidean

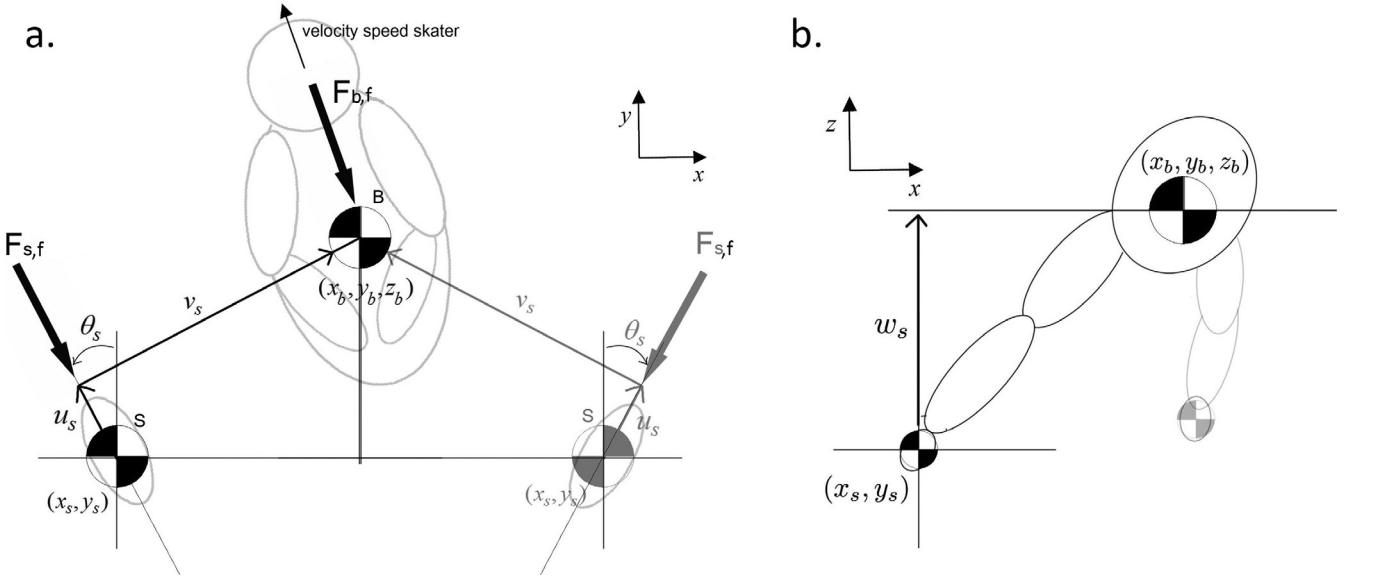

Fig. 2. Simple skater model; (a) top view of the skater; (b) rear view of skater. The skater is considered as two point masses, which are situated at the upper body (mass B) and at each skate (mass S). The position of mass B was estimated at the CoM of the HAT (head, arms and trunk). the position of mass S wat positioned at the CoM of the foot segment. The generalized coordinates are explained in Table 1.

Table 1
Clarification on the generalized coordinates.

q	Generalized coordinates
u_b	Absolute position of mass B in x-direction (global)
v_b	Absolute position of mass B in y-direction (global)
w_s	Vertical distance between the mass S and mass B
u_s	Horizontal distance between mass S and mass B in heading direction of the skate
v_s	Horizontal distance between mass S and mass B perpendicular to the heading direction of the skate
θ_s	Heading of the skate (counterclockwise)

distance in 3D space), which will be indicated as the leg extension in the remainder of this paper, and the steering angle of the skate; these are relative measures. The output of the model is the upper body motion of the skater in global space together with the forces exerted by the skates on the ice.

2.2. Generalized coordinates

The global coordinates describing the position of upper body B and skate S are,

$$\boldsymbol{x} = [\,x_b \quad y_b \quad z_b \quad x_s \quad y_s \quad \phi_s\,] \tag{1}$$

We want to express the coordination of the skater in terms of leg extension. Instead of describing the position and orientation of the body together with the constraints imposed by the joints on these coordinates $\boldsymbol{x}$ we use a minimum set of coordinates $\boldsymbol{q}$,

$$\boldsymbol{q} = [\,u_b \quad v_b \quad w_s \quad u_s \quad v_s \quad \theta_s\,] \tag{2}$$

Where $(w_s, u_s, v_s, \theta_s)$ describe the leg extension that is actively controlled by the skater and therefore serve as the input coordinates to the model (Fig. 2). The remaining coordinates (u_b, v_b) are the generalized coordinates of the upper body, which will be a result of the system dynamics. The global coordinates $\boldsymbol{x}$ can be expressed in terms of the generalized coordinates

$$\boldsymbol{x} = T(\boldsymbol{q}) \tag{3}$$

$$\begin{bmatrix} x_b \\ y_b \\ z_b \\ x_s \\ y_s \\ \phi_s \end{bmatrix} = \begin{bmatrix} u_b \\ v_b \\ w_s \\ u_b - kk \cdot \cos(\theta_s) \cdot v_s + kk \cdot \sin(\theta_s) \cdot u_s \\ v_b - \sin(\theta_s) \cdot v_s - \cos(\theta_s) \cdot u_s \\ kk \cdot \theta_s \end{bmatrix} \tag{4}$$

Where kk is the parameter introduced to distinct the alternating left active skate ($kk = 1$) and the right active skate ($kk = -1$). A derivation of these relations lead to a Jacobian matrix $\mathbf{T}$, which maps global velocities onto generalized velocities.

$$\dot{\boldsymbol{x}} = \frac{\partial T}{\partial \boldsymbol{q}}\dot{\boldsymbol{q}} = \boldsymbol{T}\dot{\boldsymbol{q}} \tag{5}$$

The matrix $\mathbf{T}$ can also be used to transform the global mass and force matrix into mass and force matrices that act on the generalized coordinates (local frame).

2.3. Unconstrained equations of motion

We first determine the unconstrained equations of motion and then add a non-holonomic constraint to the skate to restrict any lateral slip in the next section. The unconstrained equations of motion in terms of generalized coordinates according to Newton's law are then described by

$$\bar{\boldsymbol{M}} \cdot \ddot{\boldsymbol{q}} = \bar{\boldsymbol{F}} \tag{6}$$

Where $\ddot{\boldsymbol{q}}$ is the second derivative of $\boldsymbol{q}$ with respect to time. $\bar{\boldsymbol{M}}$ and $\bar{\boldsymbol{F}}$ are respectively the mass and the force matrix acting on the generalized coordinates. $\bar{\boldsymbol{M}}$ is found by

$$\overline{\mathbf{M}} = \mathbf{T}^{\mathbf{T}}\mathbf{M}\mathbf{T} \tag{7}$$

$$\boldsymbol{M} = \begin{bmatrix} m_b & 0 & 0 & 0 & 0 & 0 \\ 0 & m_b & 0 & 0 & 0 & 0 \\ 0 & 0 & m_b & 0 & 0 & 0 \\ 0 & 0 & 0 & m_s & 0 & 0 \\ 0 & 0 & 0 & 0 & m_s & 0 \\ 0 & 0 & 0 & 0 & 0 & I_s \end{bmatrix} \tag{8}$$

where m_b is the mass of B, m_s the mass of S and I_s the mass moment of inertia of S. The second reduced matrix, is the reduced force matrix $\overline{\mathbf{F}}$ which is defined as

$$\overline{\mathbf{F}} = \mathbf{T}^{\mathbf{T}}(\mathbf{f} - \mathbf{M} \cdot \boldsymbol{h}_{\mathbf{con}}) + \mathbf{Q} \tag{9}$$

where $\boldsymbol{Q}$ are the forces exerted on the local frame and $\boldsymbol{h}_{\mathbf{con}}$ are the convective acceleration terms of $\boldsymbol{x}$,

$$\ddot{\boldsymbol{x}} = \boldsymbol{T}\ddot{q} + \boldsymbol{h}_{con} \tag{10}$$

With

$$\boldsymbol{h}_{\boldsymbol{con}} = \frac{\partial \boldsymbol{T}}{\partial \boldsymbol{q} \cdot \partial \boldsymbol{q}}\dot{\boldsymbol{q}} \cdot \dot{\boldsymbol{q}} \tag{11}$$

The forces $\boldsymbol{f}$ consist of gravitational and friction forces acting on $\boldsymbol{x}$. The external forces $\boldsymbol{f}$ are described by:

$$\boldsymbol{f} = \begin{bmatrix} sin(\theta_b) \cdot F_{b,f} \\ -cos(\theta_b) \cdot F_{b,f} \\ -m_b \cdot g \\ Kk \cdot sin(\theta_s) \cdot F_{s,f} \\ -cos(\theta_s) \cdot F_{s,f} \\ kk \cdot M_s \end{bmatrix} \tag{12}$$

$F_{b,f}$ represents the air friction working on the skater. We described the air friction forces based on the study of van Ingen Schenau (1982):

$$F_{b,f} = \frac{1}{2}AC_d\rho\mathbf{v}_{xyz}^2 = k_1\mathbf{v}_{xyz}^2 \tag{13}$$

where C_d represents the drag coefficient, A the frontal projected area of the skater, ρ the air density and $\mathbf{v_{xyz}}$ the velocity of the air with respect to the skater. $F_{s,f}$ is the ice friction working on the skate, which is described using Coulomb's law of friction (De Koning et al., 1992):

$$F_{s,f} = \mu F_N \tag{14}$$

where μ is the friction coefficient and F_N is the normal force of the skate on the ice. Since the normal force is one of the outcomes of the model and μ is small, the normal force is approximated by $F_N \approx mg$ in which m the mass of the skater and g the earth gravity.

2.4. Constrained equations of motion

The acting external forces are the air frictional forces acting on the body (located at mass B) and the ice frictional forces acting on the skate. The undetermined external force acting on the skate is the constraint force perpendicular to the skate blade in the transverse plane, restraining any lateral slip of the skate. This was implemented in the model by means of a non-holonomic constraint acting in the lateral direction of the skate.

$$C_s = -sin(\theta_s) \cdot \dot{y}_s - kk \cdot cos(\theta_s) \cdot \dot{x}_s = 0 \tag{15}$$

Expressing C_s into the generalized coordinates and differentiating ones, leaves us with the equation

$$\boldsymbol{C}\ddot{q} + \boldsymbol{C}_{con} = 0 \tag{16}$$

In which $\boldsymbol{C}$ is the Jacobian of the constraints and $\boldsymbol{C}_{con}$ are the convective acceleration terms of the constraints. Adding these constraints to the total equation of motion, Eq. (5) results in:

$$\begin{bmatrix} \overline{\mathbf{M}} & \boldsymbol{C}^T \\ \boldsymbol{C} & \mathbf{0} \end{bmatrix} \begin{bmatrix} \ddot{\boldsymbol{q}} \\ \lambda \end{bmatrix} = \begin{bmatrix} \overline{\mathbf{F}} \\ -C_{con} \end{bmatrix} \tag{17}$$

where λ is the constraint force (Lagrange multiplier) acting in the lateral direction of the skate.

2.5. Finding the solution

The model is solved in two steps. First, since the parameters $(w_s, u_s, v_s, \theta_s)$ are considered as inputs and the air frictional forces acting on the upper body are assumed to be known, Eq. (14) can be reorganized in terms of known ($\boldsymbol{q}^{\mathbf{o}}$) and unknown ($\boldsymbol{q}^{\mathbf{d}}$) coordinates:

$$\begin{bmatrix} \overline{\mathbf{M}}^{\mathbf{dd}} & \overline{\mathbf{M}}^{\mathbf{do}} & C^{d^T} \\ \overline{\mathbf{M}}^{\mathbf{od}} & \overline{\mathbf{M}}^{\mathbf{oo}} & C^{o^T} \\ C^d & C^o & 0 \end{bmatrix} \begin{bmatrix} \ddot{\boldsymbol{q}}^d \\ \ddot{\boldsymbol{q}}^o \\ \lambda \end{bmatrix} = \begin{bmatrix} \overline{\mathbf{F}}^{\mathbf{d}} \\ \overline{\mathbf{F}}^{\mathbf{o}} \\ -C_{con} \end{bmatrix} \tag{18}$$

the constraint force λ and the transverse position of the upper body (u_b, v_b) can be determined by solving

$$\begin{bmatrix} \ddot{\boldsymbol{q}}^d \\ \lambda \end{bmatrix} = \begin{bmatrix} \overline{\mathbf{M}}^{\mathbf{dd}} & C^{d^T} \\ C^d & 0 \end{bmatrix}^{-1} \cdot \begin{bmatrix} \overline{\mathbf{F}}^{\mathbf{d}} - \overline{\mathbf{M}}^{\mathbf{do}} \cdot \ddot{\boldsymbol{q}}^{\mathbf{o}} \\ -C_{con} - C^o \cdot \ddot{\boldsymbol{q}}^o \end{bmatrix} \tag{19}$$

The algebraic differential equations Eq. (19) cannot be solved analytically. The equations are integrated using the classical fourth order Runge Kutta method. The integration time t_n has been chosen the sample time of the measurements ($t_n = 0.01$). The constraints are fulfilled for each integration step by a coordinate projection method (Eich-Soellner and Fnhrer (1998)). Hereby a minimization problem was formulated, concerning the distance from the predicted solution to the solution which is on the constraint surface.

With above steps, the complete set of generalized coordinates $\boldsymbol{q}$ can be determined, with which the global coordinates $\boldsymbol{x}$ can be determined analytically via the kinematic relations in (Eq. (4)). Finally, with the determined $\ddot{\boldsymbol{q}}$ and λ, the forces acting on the skate $\overline{\mathbf{F}}^{\mathbf{o}}$ can be determined analytically so that a complete two-body dynamic model of the skater has been established:

$$\overline{\mathbf{F}}^{\mathbf{o}} = [\, F_{w_s} \quad F_{u_s} \quad F_{v_s} \quad M_{\theta_s} \,] \tag{20}$$

$$\overline{\mathbf{F}}^{\mathbf{o}} = \begin{bmatrix} \overline{\mathbf{M}}^{\mathbf{od}} & \overline{\mathbf{M}}^{\mathbf{oo}} & C^o \end{bmatrix} \cdot \begin{bmatrix} \ddot{\boldsymbol{q}}^d \\ \ddot{\boldsymbol{q}}^o \\ \lambda \end{bmatrix} \tag{21}$$

Summarized the known generalized coordinates $\boldsymbol{q}^{\mathbf{o}}$, which we define as the leg extension were used as input. This was utilized to solve Eq. (19) to obtain the unknown coordinates $\boldsymbol{q}^{\mathbf{d}}$, defined as the upper body translation. The motion strategy was then used to find the forces applied on the skate, applying Eq. (21).

2.6. Data collection

To verify the model, data were collected on the indoor ice rink of Thialf, Heerenveen (the Netherlands) in 2015. Four Dutch elite speed skater were equipped with two instrumented skates, on which their individual skating shoes and blades were positioned (in full detail described in: van der Kruk et al. (2016)). The data were logged on a SD-card, with the data logger which is integrated into the instrumented skates. The skates measured the force acting in the normal and lateral direction of the local skate frame (100 Hz). The ice-frictional forces (in longitudinal direction of the skates), were expected to be smaller than the cross-talk of the force sensors and therefore estimated (Eq. (14)) (van der Kruk et al., 2016). The 3D kinetic data collection is fully described in van der Kruk et al. (2017). The skater was equipped with 23 passive markers, which were captured by twenty motion capture cameras (300 Hz) on fifty meter of the straight part of the rink. Synchronisation between the instrumented skates and the motion capture system was done via a digital start-and-end-pulse.

To estimate the COM positions of the separate segments, we used a global optimization inverse kinematics method, employing an eight rigid body model with a revolute joint in the knee, while keeping the other joints spherical (described and verified in van der Kruk et al. (2017)). The position of the mass S was estimated at the CoM of the foot; the position of mass B was estimated at

Table 2
Trials and results; In total the data of four participants were used for the verification of the model. The number of trials per participant differs, even as the number of strokes per trial. This was subject to the capturing volume and the accuracy of the motion capture system. P = participant, W = weight, T = trial, S = number of strokes in trial.

P		W	η	k1	μ	T	S	velocity	Residuals		Error							
									Rxb	Ryb	Rdxb	Rdyb	RFtot	Exb	Eyb	Edxb	Edyb	EFtot	Jmin
		(kg)						(m/s)	(m)	(m)	(m/s)	(m/s)	(N)	*e-3	*e-3	*e-3	*e-3		*e-3
A	F	70	0	0.19	0.006	1	2	9.8	0.03	0.19	0.04	0.20	111	0.726	0.125	0.631	0.495	0.011	0.065
						2	3	10.0	0.02	0.10	0.02	0.12	130	0.531	0.013	0.291	0.219	0.019	0.065
B	F	65	0	0.18	0.006	1	2	8.7	0.02	0.09	0.02	0.13	83	0.307	0.026	0.192	0.316	0.011	0.046
						2	3	9.5	0.01	0.05	0.02	0.14	94	0.196	0.004	0.203	0.361	0.01	0.034
						3	2	9.9	0.04	0.33	0.04	0.24	88	0.679	0.238	0.468	0.803	0.011	0.052
						4	2	9.9	0.04	0.32	0.04	0.29	121	1.158	0.28	0.585	1.172	0.017	0.094
C	M	76	0	0.14	0.006	1	2	10.3	0.03	0.16	0.03	0.15	54	0.418	0.054	0.303	0.303	0.006	0.029
						2	2	11.1	0.03	0.15	0.03	0.16	47	0.339	0.039	0.199	0.288	0.005	0.024
						3	2	11.2	0.03	0.09	0.03	0.15	62	0.33	0.017	0.293	0.23	0.007	0.032
						4	2	11.2	0.02	0.09	0.02	0.12	65	0.258	0.014	0.199	0.165	0.008	0.036
						5	2	11.8	0.03	0.13	0.03	0.18	72	0.756	0.046	0.495	0.332	0.008	0.051
						6	3	12.4	0.02	0.13	0.03	0.14	80	0.247	0.02	0.354	0.179	0.008	0.034
						7	2	12.8	0.02	0.15	0.03	0.19	83	0.6	0.056	0.477	0.278	0.009	0.055
D	M	81	0	0.14	0.006	1	2	10.5	0.03	0.27	0.03	0.21	72	0.294	0.097	0.302	0.515	0.007	0.027
						2	2	10.7	0.04	0.39	0.05	0.31	82	0.508	0.222	0.653	0.926	0.007	0.034
						3	2	10.8	0.04	0.32	0.04	0.25	135	0.556	0.17	0.444	0.673	0.017	0.073
						4	2	11.1	0.03	0.24	0.03	0.22	132	0.432	0.106	0.389	0.513	0.014	0.066
						5	2	12.3	0.02	0.21	0.04	0.23	128	0.471	0.115	0.43	0.408	0.011	0.067

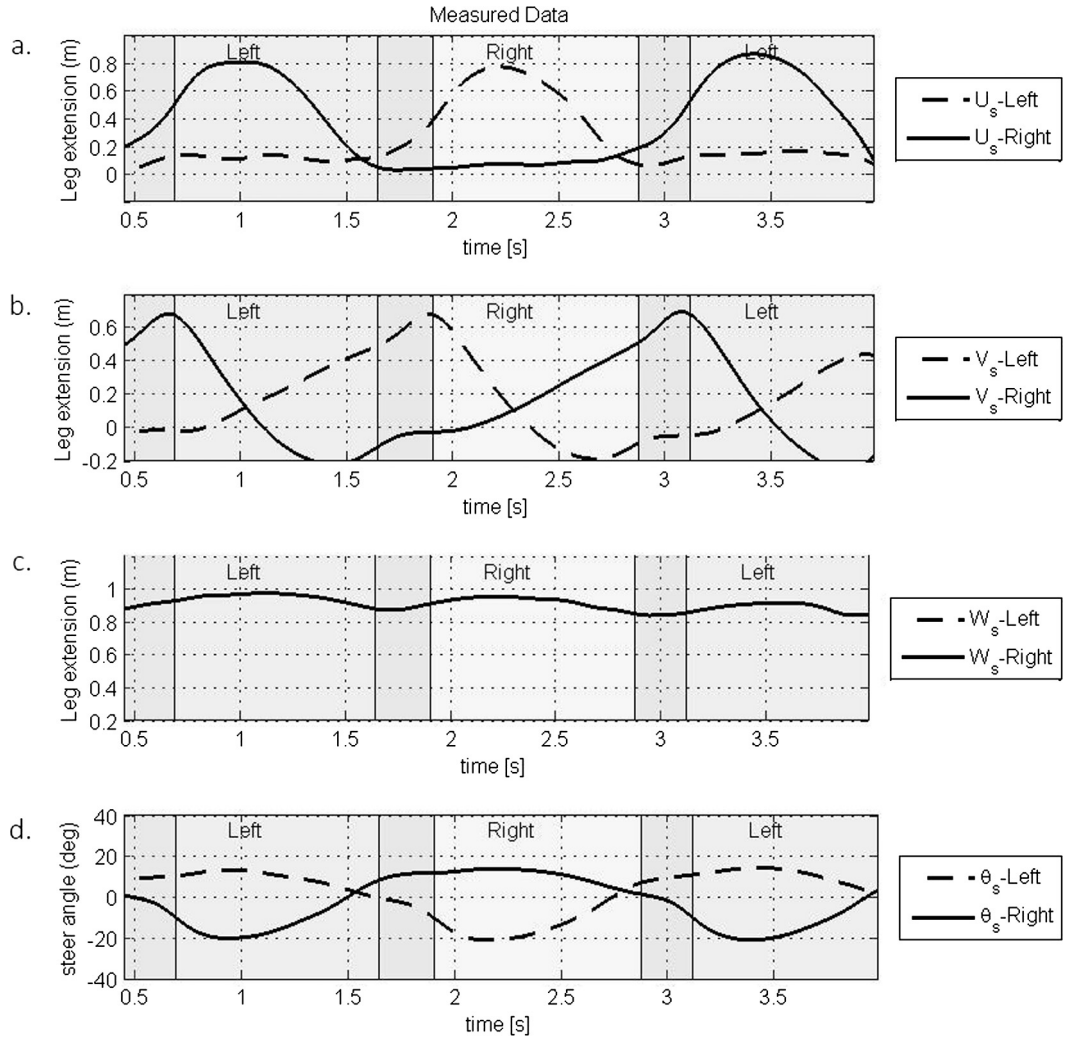

Fig. 3. Typical example of the (filtered) measured leg extension of a speed skater. The text indicates which skate is active (on the ice). The double stance phase – where both skates are on the ice – is indicated by the vertical lines and the dark grey area.

the CoM of HAT (which is head, arms and trunk). Since mass B is much larger than the point masses at the skates, we initially set the mass distribution coefficient (η) to zero for the verification of the model, so that all bodyweight is located at mass B (Garcia, Chatterjee, Ruina, & Coleman, 1998). Since the skate can only glide in line with the blade, the steer angle was determined by the velocity vectors of the skates.

Skaters familiarized themselves with the equipment before the start of the test. The test was divided into three parts, each at a different velocity, which each consisted of skating three laps at a constant velocity. Skaters were asked to skate at a self-chosen velocity, corresponding to the low (70%), medium (80%), and high (90%) intensity, something they are familiar with in training. Due to the complexity of the measurements – foremost the large size of the capturing volume – not all datasets were applicable for verification. In total 28 trials of the four participants were recorded, of which 18 data sets consisting each of one straight part with several strokes (in total 39 strokes) at speeds varying from 8.5-12.3 m/s were complete and used for the verification of the model (Table 2). Of participant A, only data at low intensity was applicable for verification. In the remainder of this paper we refer to the trials by the participant character and trial number, e.g. C2 is participant C, trial 2.

2.7. Model verification

The purpose of the model verification is to quantify the error between the simulated data and the measured forces and positions. Analysis of the model error is performed similar to the method of Cabrera et al. (2006). This method constructs two measures, first the residuals, defined as

$$R(y_j) = \frac{1}{N}\sum_{i=1}^{N}|\tilde{y}_{ij} - y_{ij}| \tag{22}$$

in which $\tilde{y}_{ij}$ is the simulated value of a variable, y_{ij} the measured value of a variable and N is the number of samples. Second, a measurement error Jmin independent of scales and units:

$$E(y_j) = \frac{1}{N}\sum_{i=1}^{N}\frac{(\tilde{y}_{ij} - y_{ij})^2}{\bar{y}_j^2} \tag{23}$$

$$\mathrm{J_{min}} = \frac{\sum_{j=1}^{M}E(y_j)}{N} \tag{24}$$

In which $\bar{y}_j$ is the characteristic value of the variable, N is the number of samples and M is the number of residuals. The errors of the upper body positions (x_b, y_b), the upper body velocity

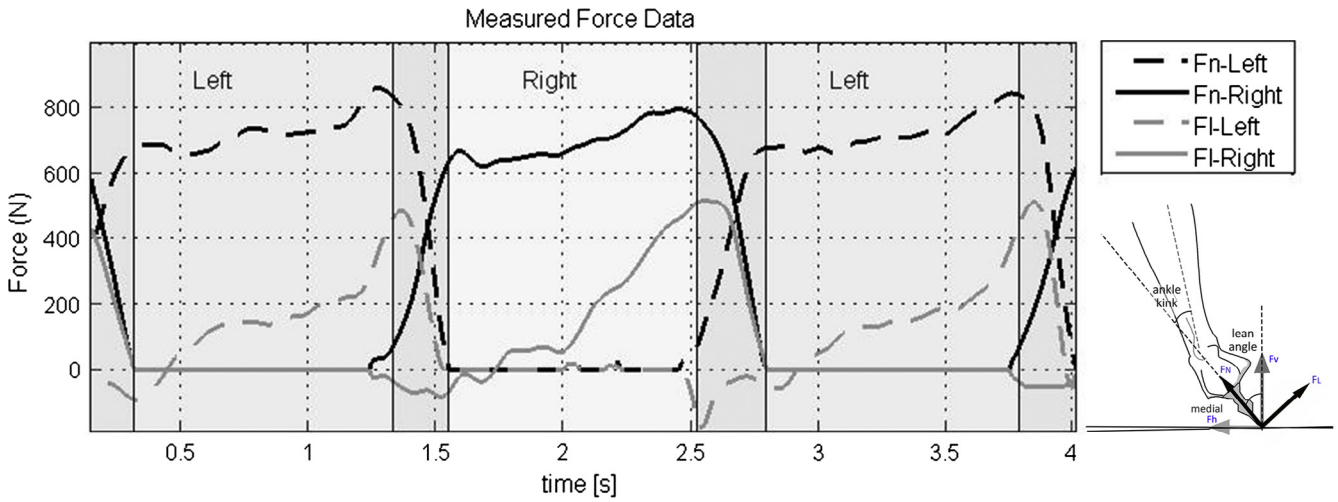

Fig. 4. Typical example of the (filtered) measured normal (Fn) and lateral (Fl) forces of a speed skater. The text indicates which skate is active (on the ice). The double stance phase – where both skates are on the ice – is indicated by the vertical lines and the dark grey area.

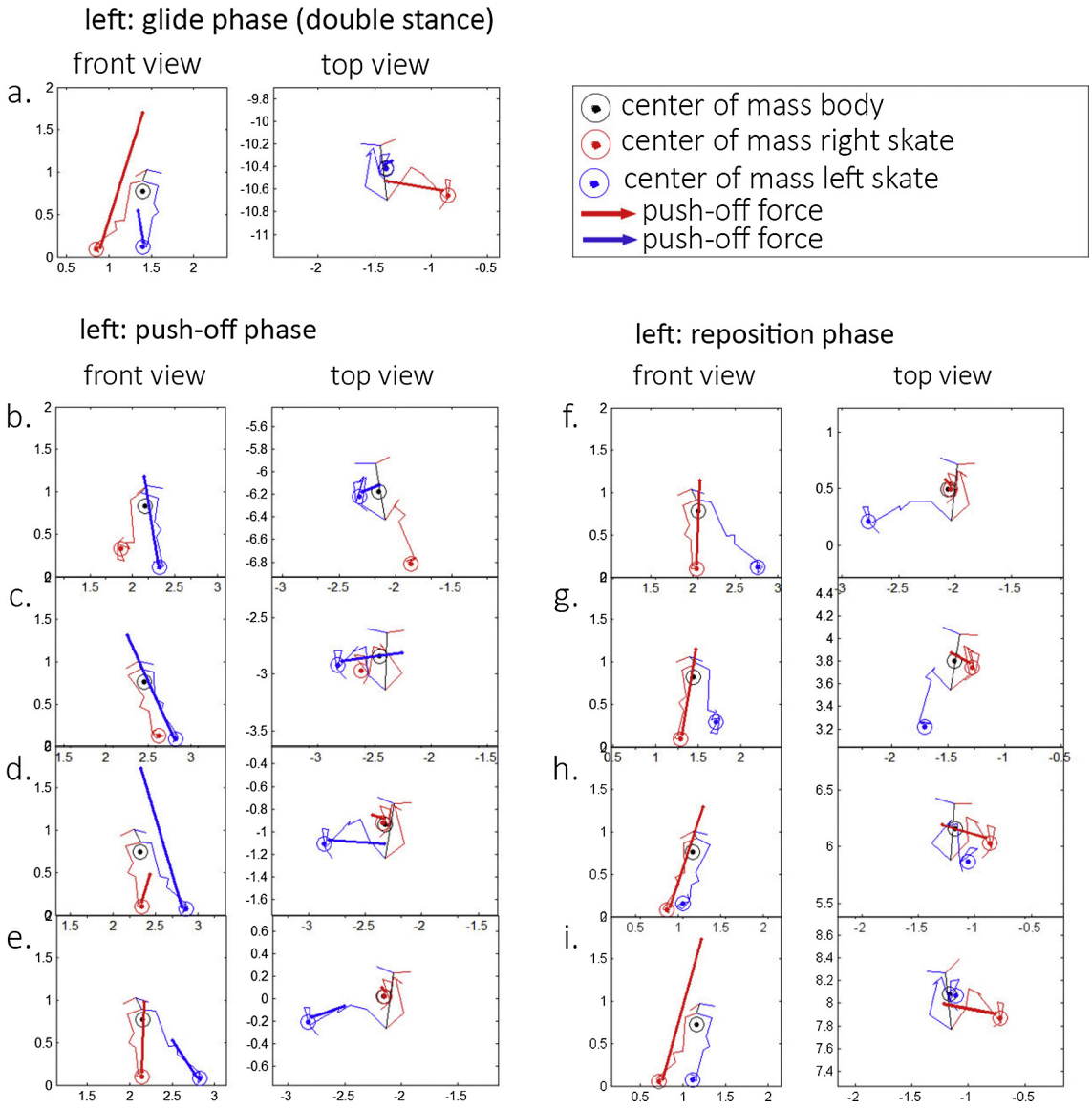

Fig. 5. Position of the skates relatively to the center of mass throughout the speed skating stroke. Focus is on the left (blue) skate. The arrows indicate the force applied on the skate. When the skate does not have an arrow, there is no force on the skate, meaning that it is lifted from the ice (repositioning). (For interpretation of the references to colour in this figure legend, the reader is referred to the web version of this article.)

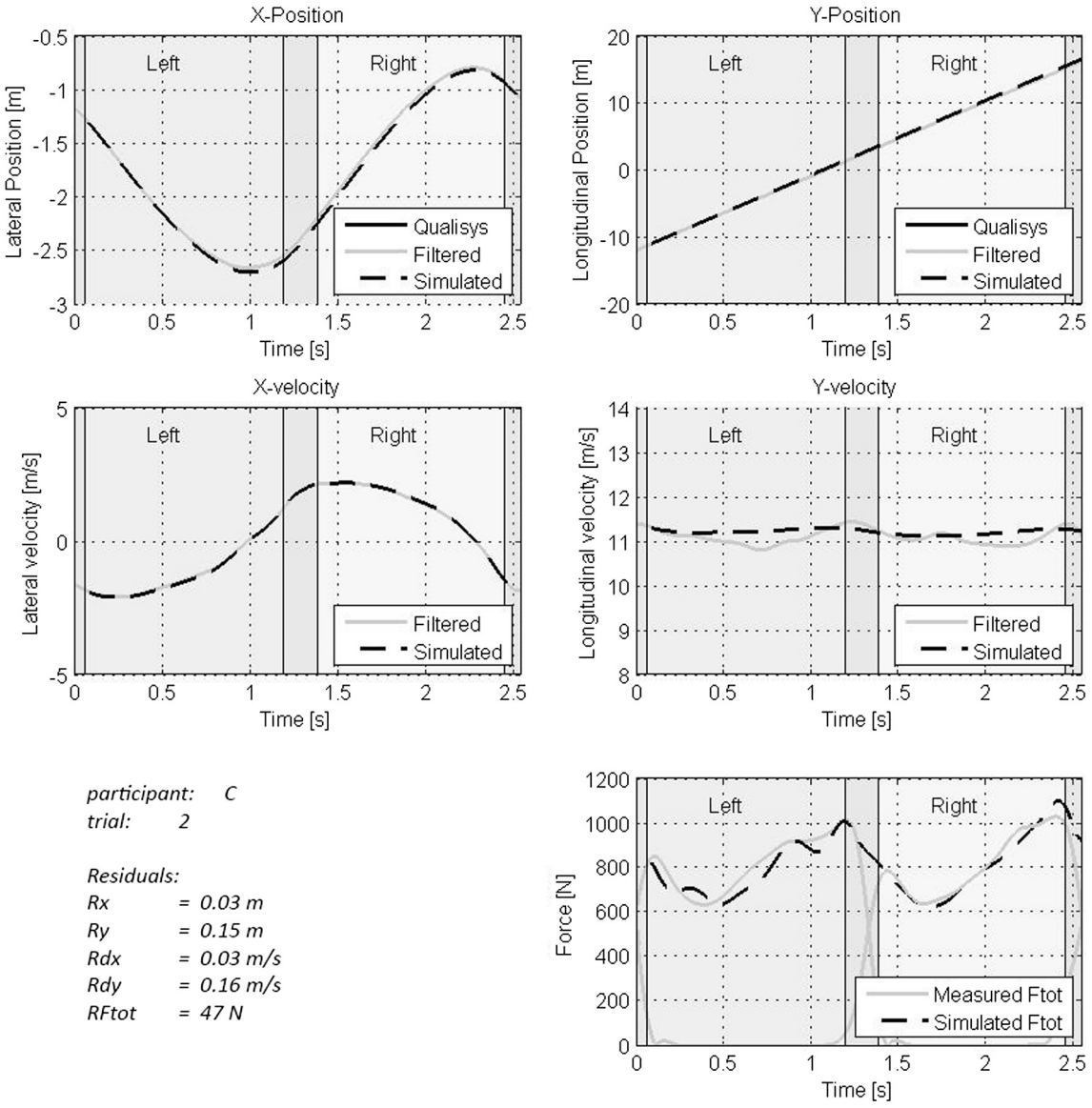

Fig. 6. Results on the measured and model data of the best fit of the model (C2).

($\dot{x}_b$, $\dot{y}_b$) and the magnitude of the force (F_{tot}) are taken into account. The peak to peak values of the upper body positions, average value of the body velocity in forward direction, peak value of the velocity in sideward direction and the maximum local measured normal peak force are used as the characteristic values of the parameters.

3. Results

3.1. Measured data

An example of the measured leg extensions of both left and right strokes are shown in Fig. 3. The motion pattern is similar for the left and the right stroke. For better comprehension of the movement, Fig. 5 shows a motion plot of the skater. At the start of the stroke (the glide phase), the skate is positioned on the lateral opposite side of mass B, indicated by the negative v_s, and almost under mass B in the longitudinal direction, indicated by a close-to-zero u_s (Fig. 3a,b, Fig. 5a). The skate is then moved sideways (the push off phase) whereby v_s increases up to about 0.7 m (Fig. 3b, Fig. 5b-e). Only in the last part of the push-off (Fig. 5d, e), the skate is moved backward from the upper body mass, indicated by the increase of u_s (Fig. 3a). In the repositioning phase the skate is retracted to the upper body, thereby first moving the skate sideward (Fig. 5f,g) and then forward (Fig. 5h,i). The vertical distance between the skate and the upper body increases and decreases within the stroke, describing a sine wave like trajectory in the transverse plane, during speed skating the straights (Fig. 3c). The measured normal and lateral forces were similar to previously published skating data (van der Kruk et al., 2016) (Fig. 4).

3.2. Model data

The simple skater model mimics the skaters observed motion and forces well as can be concluded from the results presented in Table 2, where the residuals and the Jmin values are shown in column 9–25. We selected the best fit (C2, *Jmin* = 0.024) and the worst fit (B4, *Jmin* = 0.094) to present in Fig. 6 and Fig. 7. The model errors found in the verification process proofed to be unrelated to the velocity in the trial or the participant (mass and technique).

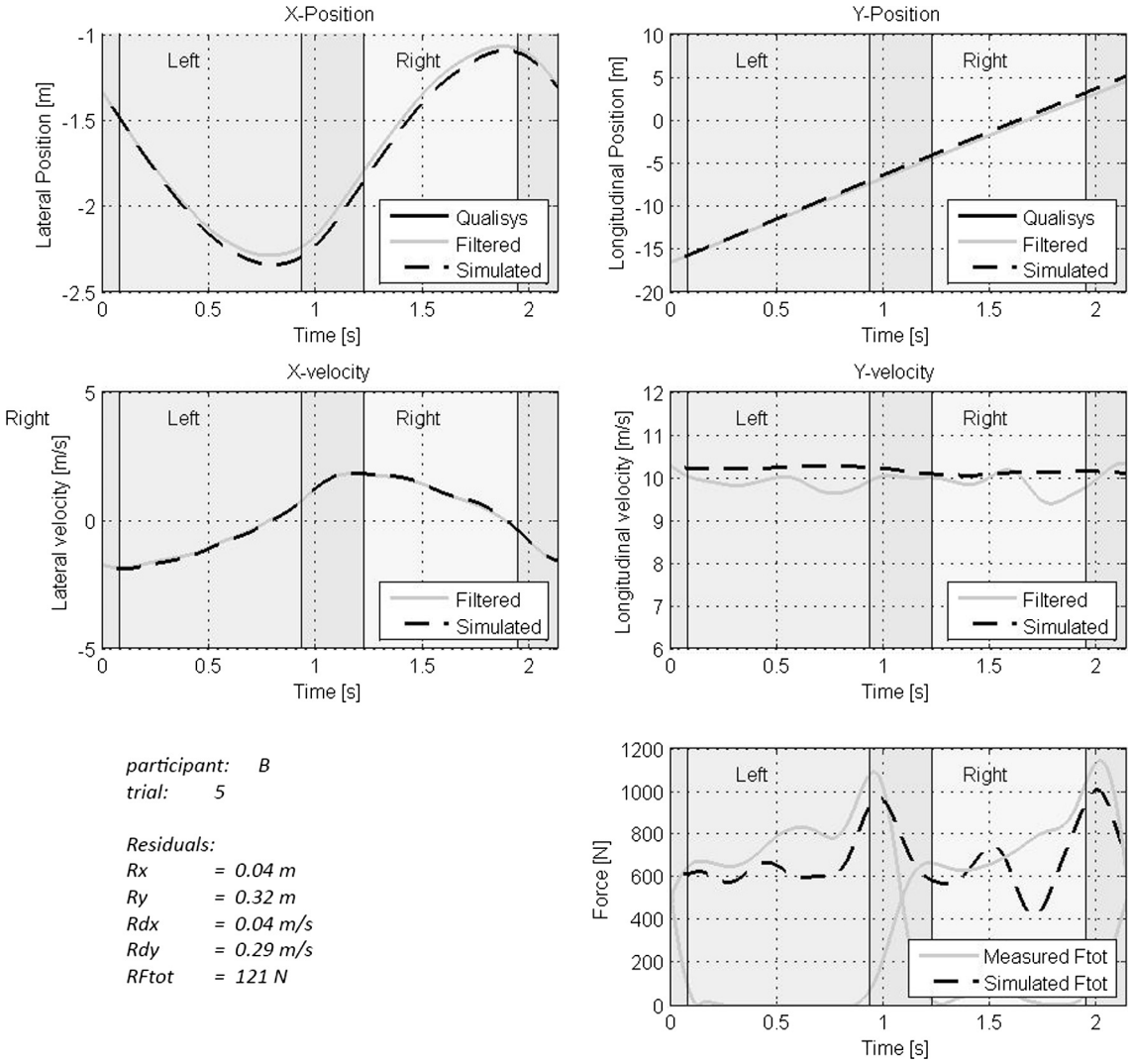

Fig. 7. Results on the measured and model data of the worst fit of the model (B4).

The model performs best for the simulation of position and velocity of mass B with a maximal residual of 0.04 m in x- and 0.39 m in y-position (distance covered is 33 m) and 0.05 m/s for x-velocity (D2). Maximum residual in y-velocity is 0.31 m/s; the model simulates the average y-velocity over a stroke correctly, but lacks to simulate the occurring fluctuations within a stroke; We will elaborate on this in the discussion.

Force data have the least accurate fit and were underestimated in each test. The minimum force residual found is 47 N (C2), the maximum residual found is 135 N (D3) (peak forces here are 1000 N and 1250 N respectively). The success of the simulation is independent of subject and unrelated to the velocity of the skater and the number of strokes within a trial.

4. Discussion

The simplified model of a skater proved to mimic the observed forces and motions of a speed skater well. The model can therefore be used to further investigate variables in the skating motion. For this, the input of the model, the leg extension, can be optimized to obtain a maximal forward velocity of the upper body. The leg extension is an indirect measure of the knee flexion-extension, the ankle eversion, the lean angle of the skate, hip abduction and the steering of the skate. Anatomic restrictions and maximum leg extension velocity would be part of the constraints in such an optimization procedure.

The model errors found in the verification process proofed to be unrelated to the velocity in the trial or the participant (mass and technique). The differences found between trials are therefore related to the accuracy of the measured data, and the correctness of the estimated data, e.g. air friction; this is further discussed in section 4.2. The model does have two general limitations; first the forward velocity, where the model showed to be incapable of simulating the within-stroke fluctuations, and second the underestimation of the forces. Since both limitations also provide insight into the skating mechanics, they are discussed next.

4.1. Swing leg error

The fluctuation – or dip – in the measured forward velocity of mass B is probably caused by the swinging leg in repositioning, which was neglected in our simplified model. To get a rough idea on the magnitude of the necessary acceleration of the swinging leg to cause the deceleration and acceleration of the mass B, we simplified the system again in two masses; assume this time that mass 1 (m_1) is the swinging leg and mass 2 (m_2) is the remaining body and the sum of the forces is zero. Then, with the momentum conservation principle, we know that:

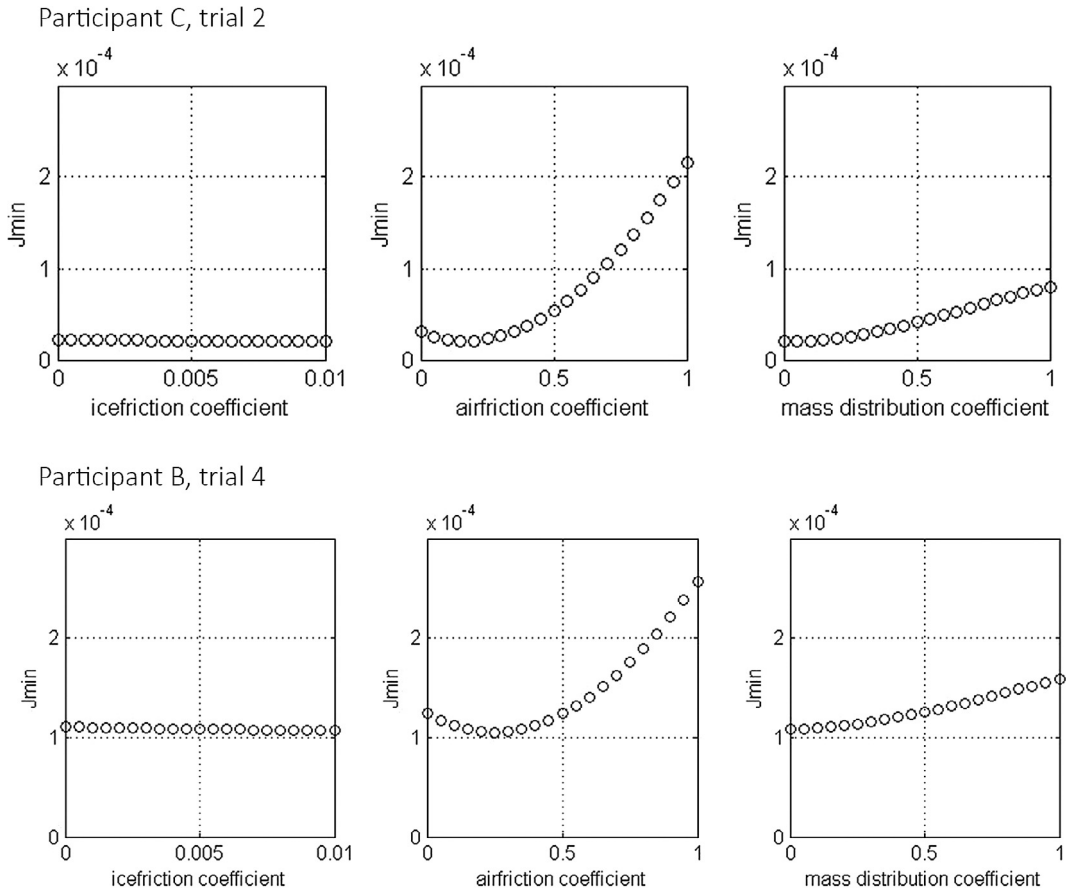

Fig. 8. Results on the sensitivity analysis for C2 and B4.

$$m_1\ddot{x}_1 + m_2\ddot{x}_2 = 0 \quad (25)$$

From Dumas et al. (2007) we know that the mass of one foot, one shank and one thigh is 0.161 times the body mass. So the ratio for the acceleration of the swinging leg and the rest of the body should be around 0.192; In the data the acceleration of the mass B is around -2 m/s^2, which requires a 10 m/s^2 acceleration of the swinging leg. This swinging leg reaches accelerations of 12 m/s^2 and could therefore well explain the fluctuation in velocity within the skating stroke. This is an interesting fact, while the swinging leg was, up to now, always neglected in speed skating analyses.

Other simplifications that influence the forward velocity estimation are the negligence of arm movements, body-segment rotations, and change in frontal area (air friction). However their influence is not as large as the one inflicted by the swinging leg. For the arm-movements this was determined in a simple post hoc analysis, by comparing the model fit of the skaters performing an arm swing (skaters A, B, C) to the skater which kept his arms on his back (skater D) (based on video analysis). Table 2 shows us that the model fit of skater D is not better compared to the others, so the HAT segment assumption cannot be of large influence on the model fit.

For the underestimation of the measured force, the cause is less straightforward, while we expect that it is a conjunction of simplifications. The model assumes that all force is directed at mass B, the HAT segment. However, in reality the push-off of the skater is not that utter efficient; ankle eversion and damping in the leg cause that not all the force we measured at the skate is directly addressed to mass B. Some of this is lost to segment rotations or friction, both of which were not accounted for in the model. Furthermore, we neglected the double stance phase, in which both skates are on the ice. The neglected skate – which starts in the glide phase – does not add much force, but will increase the ice friction (although small), and, when placed incorrectly, can cause a force detrimental to the forward velocity (van der Kruk et al., 2016).

4.2. Sensitivity analysis

In the model, three inputs were kept constant: the mass distribution, the ice friction coefficient and the air friction coefficient (k1). The sensitivity of the model to these mechanical constants can be determined by changing one of them while keeping the remaining constants fixed. The results of this sensitivity analysis for again B4 and C2 are shown in Fig. 8. The ice friction coefficient has least impact on the fit, indicating that ice friction has relatively little impact on the skating velocity. The mass distribution coefficient has more impact, but was zero in our verification process and thus close to optimal.

The model is most sensitive to the air friction coefficient (k1), which was expected; after all there are power models purely based on this air friction (de Koning et al., 2005). For the verification process, k1 was kept at a constant value based on previous literature (van Ingen Schenau, 1982). We could, however, also determine the air friction coefficient via optimization of the model, fitting the model to the measured data. The sensitivity analysis shows that the k1 used in C2 (our best fit) is close to optimal (0.14), while the k1 used in B4 - our worst fit - could be improved by increasing the coefficient from 0.18 to 0.25. Adjusting k1 in B4, benefits the estimated y-position and velocity most, while their residuals are respectively reduced from 0.32 m to 0.23 m and 0.29 m/s to 0.23 m/s (a 27% and 21% improvement). The model could therefore

benefit from an improved estimation, or measurement, of air frictional forces (Terra et al., 2017).

5. Conclusion

We modelled a speed skater as two point masses, one at the foot and one at the upper body, and used the leg extension (the changing distance between these two masses) and the steering of the skate as input for the model. Verification shows that the model mimics the observed forces and motions well. The model is most accurate for the position and velocity estimation (respectively 1.2% and 2.9% maximum residuals). It is least accurate for the force estimations which, due to simplifications, are underestimated with 4.5–10%. The model can be used to further investigate variables in the skating motion. For this, the input of the model, the leg extension, can be optimized to obtain a maximal forward velocity of the upper body.

Acknowledgement

The authors express their gratitude to Frida Bakkman, Daniel Thompson, Erik Westerström and Marcus Johansson of Qualisys, Wouter van der Ploeg of the KNSB, Andre Zschernig of the company Moticon and Frédérique Meeuwsen, Niels Lommers and Jos Koop of the TU Delft and the Hague university of applied sciences for their help and support during the measurements. Also we express gratitude to Thialf for giving us the opportunity of overnight measurements at their rink. Furthermore we thank dr. D.M. Fintelman for her work on this project. This study was supported by the NWO-STW under grant 12870.

References

Allinger, T.L., Bogert, A.J., 1997. Skating technique for the straights based on the optimization of a simulation study. Med. Sci. Sports Exerc. 29, 279–286.

Bruzzo, J., Schwab, A.L., Valkeapää, A., Mikkola, A., Ohtonen, O., Linnamo, V., 2016. A simple mechanical model for simulating cross-country skiing, skating technique. Sports Eng. 19 (2), 91–104.

Cabrera, D.D., Ruina, a., Kleshnev, V., 2006. A simple 1+ dimensional model of rowing mimics observed forces and motions. Hum. Mov. Sci. 25 (2), 192–220. http://dx.doi.org/10.1016/j.humov.2005.11.002.

De Koning, J.J., De Groot, G., Van Ingen Schenau, G.J., 1992. Ice friction during speed skating. J. Biomech. 25 (6), 565–571. http://dx.doi.org/10.1016/0021-9290(92)90099-M.

de Koning, J.J., Foster, C., Lampen, J., Hettinga, F., Bobbert, M.F., 2005. Experimental evaluation of the power balance model of speed skating. J. Appl. Physiol. 98 (1), 227–233. http://dx.doi.org/10.1152/japplphysiol.01095.2003.

Dumas, R., Chèze, L., Verriest, J.P., 2007. Adjustments to McConville et al. and Young et al. body segment inertial parameters. *J. Biomech.* 40 (3), 543–553. http://dx.doi.org/10.1016/j.jbiomech.2006.02.013.

Eich-Soellner, E., Führer, C., 1998. Numerical methods in multibody dynamics (vol. 45). Springer.

Fintelman, D.M., Den Braver, O., Schwab, A.L., 2011. A simple 2-dimensional model of speed skating which mimics observed forces and motions. In Multibody dynamics, ECCOMAS Thematic Conference, Brugge, Belgium. (vol. 511).

Garcia, M., Chatterjee, A., Ruina, A., Coleman, M., 1998. The simplest walking model: stability, complexity, and scaling. Journal Biomechanical Engineering 120 (2), 281–288.

Otten, E., 2003. Inverse and forward dynamics: models of multi-body systems. Philosophical Transactions of the Royal Society of London B: Biological Sciences 358, 1493–1500.

Terra, W., Sciacchitano, A., Scarano, F., 2017. Aerodynamic drag of transiting objects by large-scale tomographic-PIV. Exp. Fluids 58 (7), 83.

van der Kruk, E., den Braver, O., Schwab, A.L., van der Helm, F.C.T., Veeger, H.E.J., 2016. Wireless instrumented klapskates for long-track speed skating. Journal of Sports Engineering 19 (4), 273–281. http://dx.doi.org/10.1007/s12283-016-0208-8.

van der Kruk, E., Schwab, A.L., van der Helm, F.C.T., Veeger, H.E.J., 2017. Getting in shape: reconstructing three-dimensional long-track speed skating kinematics by comparing several body pose reconstruction techniques. *Under Review at Journal of Biomechanics*.

van der Kruk, E., Veeger, H.E.J., van der Helm, F.C.T., Schwab, A.L., 2015. Two Body Dynamic Model for Speed Skating Driven by the Skaters Leg Extension. In icSports conference 2015.

van Ingen Schenau, G.J., 1982. The influence of air friction in speed skating. J. Biomech. 15 (6), 449–458. http://dx.doi.org/10.1016/0021-9290(82)90081-1.

Van Ingen Schenau, G.J., 1981. A power balance applied to speed skating. PhD. thesis. Vrije Universiteit Amsterdam.